Energy & Environmental Science

A Low Temperature Unitized Regenerative Fuel Cell Realizing 60% Round Trip Efficiency and 10,000 Cycles of Durability for Energy Storage Applications

Journal:	*Energy & Environmental Science*
Manuscript ID	EE-ART-11-2019-003626.R3
Article Type:	Paper
Date Submitted by the Author:	12-Feb-2020
Complete List of Authors:	Regmi, Yagya; Lawrence Berkeley National Laboratory, Peng, Xiong; Lawrence Berkeley National Laboratory Fornaciari, Julie; Lawrence Berkeley National Laboratory; University of California Berkeley, Chemical and Biomolecular Engineering Wei, Max; Lawrence Berkeley National Laboratory Myers, Deborah; Argonne National Laboratory, Chemical Sciences and Engineering Division Weber, Adam; Lawrence Berkeley National Laboratory, Energy Technologies Area Danilovic, Nemanja; Lawrence Berkeley National Laboratory, Energy Storage and Distributed Resources

A Low Temperature Unitized Regenerative Fuel Cell Realizing 60% Round Trip Efficiency and 10,000 Cycles of Durability for Energy Storage Applications

Yagya N. Regmi[1], Xiong Peng[1], Julie C. Fornaciari[1,2], Max Wei[3], Deborah J. Myers[4], Adam Z. Weber[1], Nemanja Danilovic[1,*]

[1] Energy Storage and Distributed Resources Division, Lawrence Berkeley National Laboratory, Berkeley, CA, 94720.

[2] Department of Chemical and Biomolecular Engineering, University of California Berkeley, Berkeley, CA, 94720

[3] Energy Analysis and Environmental Impacts Division, Lawrence Berkeley National Laboratory, Berkeley, CA, 94720.

[4] Chemical Sciences and Engineering Division, Argonne National Laboratory, Lemont, IL, 60439

* ndanilovic@lbl.gov

1. Broader context

An electrolyzer and fuel cell together form an electrochemical battery with a storage capacity limited by storage media, not the conversion device. A proton-exchange membrane (PEM) system that is used to store and release chemical energy from hydrogen molecule also has the added advantages of extended storage life and portability. However, electrochemical energy conversion using two discrete PEM devices (fuel cell and electrolyzer) adds significant capital costs. Unitized regenerative fuel cells (URFC) can reduce the price if a single unit can achieve high roundtrip efficiencies (RTE). Thus, exploring the operational RTE limits of URFCs is essential. We assess the RTEs of PEM-based URFCs in an unconventional configuration where

hydrogen oxidation and oxygen evolution occur on one electrode, and oxygen reduction and hydrogen evolution on the other. We also show that this configuration has the potential to operate at higher current densities and RTEs than traditional URFCs, where both oxygen reactions take place on one electrode and both hydrogen reactions on the other. These assessments will provide guidelines for future investigations to further optimize the system and RTEs via materials and system innovations, ultimately bringing down the unit price of the electrochemical generation and utilization of hydrogen.

2. Abstract

Unitized regenerative fuel cells (URFC) convert electrical energy to and from chemical bonds in hydrogen. URFCs have the potential to provide economical means for efficient long-term, seasonal, energy storage and on-demand conversion back to electrical energy. We first optimize the catalyst layer for discrete electrolyzer and fuel cell and then configure the URFC. Two possible configurations of URFCs are compared, which emphasize the advantages of the unconventional *constant-electrode (CE)* URFC over the traditional *constant-gas (CG)* configuration. We also study the stability via accelerated stress tests (ASTs) and demonstrate steady state operation in a daily cycle for day to night energy shifting. The goal is to identify a competitive configuration for URFCs, and demonstrate it in terms of upper limit of round trip efficiencies (RTEs). From the investigations, the optimum composition of the URFC anode catalyst layer is 90 at% Ir-black balanced by Pt-black for both CE and CG configurations. At 80 °C and 1 A/cm^2, the optimized CE URFC achieves 58 and 61% RTE with air and O_2 as the reductant gases, respectively. We then evaluated the differences in durability using an AST over 10k charge-discharge cycles; the results reveal that the wider potential window at the anode in

CE (0.05-1.55 V) has minimal effect on catalyst layer stability compared to CG (0.55-1.55 V). Furthermore, there was no degradation up to the range of 2k-5k cycles; beyond that the fuel cell (discharge) performance degraded while the electrolyzer (charge) performance was still stable. The observations here indicate substantial potential to employ URFCs as efficient and cost-effective bidirectional energy-conversion devices within energy storage and utilization systems after appropriate technological and operational optimizations.

3 Introduction

Energy storage is increasingly important for electrical grid resiliency as intermittent and variable energy sources intermingle on the electrical grid.[1] There are numerous energy and time domains that require the appropriate energy-storage technology at a low price point. These solutions include technologies whose deployment is regionally dependent, such as hydropower and air compression, that can depend on the presence of geological features.[2, 3] In contrast, electrochemical-based storage technologies can be readily deployed without geological constraints, including lithium-ion batteries, flow batteries, and electrolyzers (EL).[4] The capital and operational expenditures (capex and opex, respectively) of each technology dictate the amount and timescale over which the system can store energy.[5] For example, even though the cost of lithium batteries has come down tremendously due to the emerging battery-electric vehicle industry, the cost to store more than four hours of energy makes them prohibitive for longer duration energy-storage applications.[6] For longer time domains, flow batteries and hydrogen storage have been proposed due to the ability to decouple the energy-conversion and the energy-storage components of the system, since storage tanks can be used to hold electrolyte or hydrogen (H_2), respectively. Hydrogen, produced from electricity and water in an electrolyzer

(EL) is considered, in particular, as a versatile long-term and seasonal energy storage option. The hydrogen can then be used for heat generation, transportation, chemical feedstock or converted back to electricity using a fuel cell (FC), as outlined in the Department of Energy's H2@Scale initiative.[7] The EL and FC devices together constitute a H-ion battery, charging the H^+ ions into H_2 using electricity, and discharging the stored H_2. Conventionally, this H-ion battery is called a discrete regenerative fuel cell (RFC). When the EL and FC functionalities are combined in one device, the device is termed a unitized regenerative fuel cell (URFC). While RFCs or URFCs have conventionally been used or promoted for use in limited payload applications such as unmanned vehicles,[8] the emerging energy landscape demands cost-competitive solutions for various energy-storage scenarios.[5] The advantage of URFC over RFCs is the reduction in capex due to the minimization of cell components from two stacks into one. This paper aims to demonstrate the upper limit of roundtrip efficiency, durability, and the resulting opex of the URFC in order to determine the energy/time domain that would make the URFC cost competitive with other energy-storage technologies.

An URFC (Figure 1), consists of a membrane electrode assembly (MEA) that contains an ion-conducting membrane, typically a H^+-conducting perfluorosulfonic-acid membrane, which separates the electrodes that perform the electrocatalysis (catalyst layer) and gas or liquid transport (gas diffusion or porous transport layers).[9] During charge (EL mode), the oxygen-evolution reaction (OER) occurs at the anode and the hydrogen-evolution reaction (HER) at the cathode. During discharge (FC mode), the hydrogen-oxidation reaction (HOR) occurs at the anode and the oxygen-reduction reaction (ORR) at the cathode. An URFC requires that each electrode is bifunctional in order to sustain both modes of operation. Such bifunctionality can be

accomplished in two configurations: *constant-gas* (CG) or *constant-electrode* (CE). In the CG configuration, the URFC consists of an oxygen electrode (ORR/OER) and a hydrogen electrode (HOR/HER) (Figure 2).[10] The advantages of the CG configuration are that H_2 and O_2 mixing is avoided, and fast switching times between charge and discharge are possible. The disadvantages have historically been that the two most thermodynamically, kinetically, and transport-limited reactions, the ORR and OER, are combined on the same side of the cell resulting in a confluence of inefficiencies. In the CE configuration, the URFC consists of an anode (HOR/OER) and a cathode (ORR/HER) and the gases present on the anode and cathode are switched between EL and FC modes.[11] This configuration has distinct advantages in improving the transport of O_2 and kinetics of the ORR by optimizing the cathode catalyst and gas-diffusion layers (GDLs), while taking advantage of the facile HOR on the anode side, allowing for a reduction in catalyst loading and improved OER kinetics as well. The disadvantages of this configuration are that each electrode experiences a wider range of potentials when transitioning between FC and EL modes, which can cause higher rates of materials degradation, limiting device lifetime, and that there is a need to engineer safe transitions between charge and discharge modes to avoid mixing of oxygen and hydrogen.

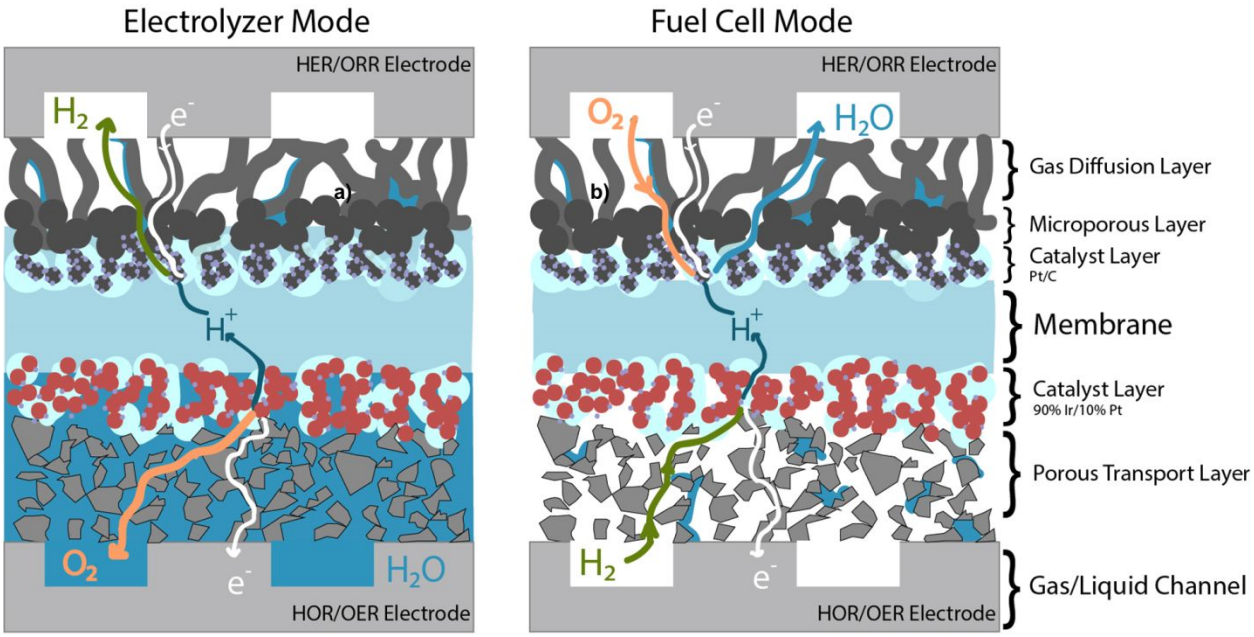

Figure 1. Schematic of a Unitized Regenerative Fuel Cell membrane electrode assembly operating in the constant electrode (CE) configuration. We note the presence of water during electrolysis, and the condensation of water vapor during fuel cell mode within the porous transport layer.

While CG mode has been studied in the literature, there is a dearth of such investigations into CE mode operation, especially with respect to optimizing the membrane electrode assembly for roundtrip efficiency (RTE) and durability. Furthermore, the application of URFCs has largely been limited to restricted payload vehicles; thus there is an absence or discussion of applications in the energy-storage field. There are several review papers that summarize recent progress.[12-16] Several studies have focused on investigating and analyzing component performance and system efficiencies for URFCs.[8, 17, 18] However, the bulk of the focus is on development of CG ORR/OER bifunctional catalyst layers.[19-23] Omrani and Shabani presented a comprehensive review of GDLs from the perspective of URFC system requirements.[24] Ito et al., on the other hand, evaluated the efficiency of a CG mode URFC at both system and stack level.[17]

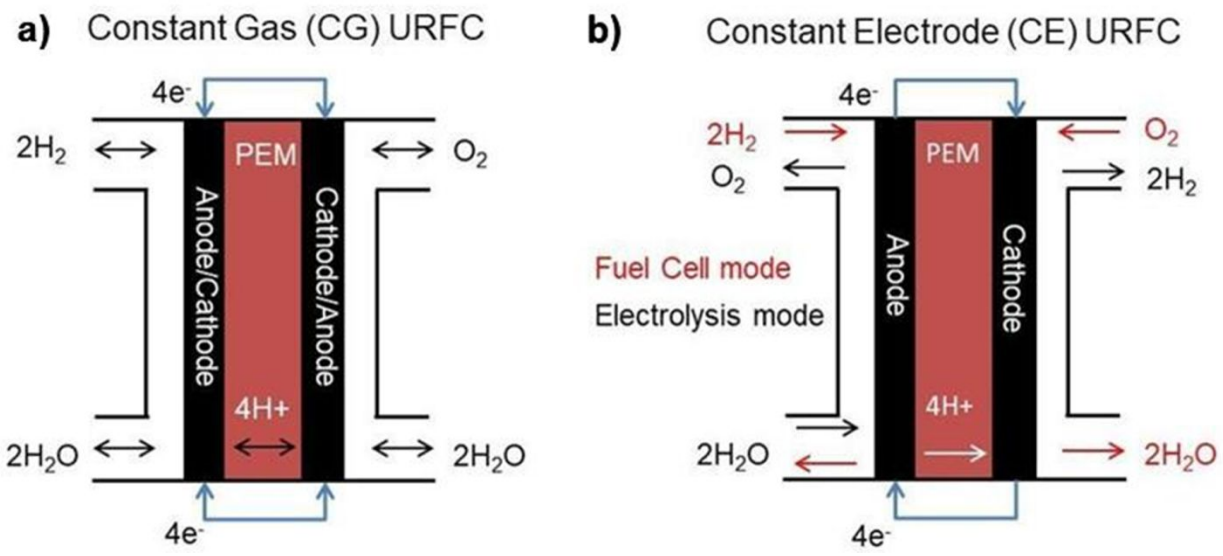

Figure 2. Schematic of two different URFC operating configurations: a) Constant Gas (CG) and b) Constant Electrode (CE).

There is a lack of studies in the URFC literature on the following topics: 1) design of URFC for optimal efficiency, 2) efficiency comparison of CE and CG configurations, and 3) design of URFCs for energy-storage applications. Our approach is to make the case for URFCs as devices for energy storage for durations longer than 4 h by redesigning the URFC MEA with state-of-the-art materials and approaches currently used in FC and EL research. The aim is to identify a competitive configuration for a unitized regenerative fuel cell in terms of upper limit of RTE, while also demonstrating the mode cycling durability. We first tune the optimal Pt/Ir ratios under discrete FC and EL conditions before combining them into a URFC MEA and comparing CE and CG modes. We also demonstrate how different components of the FC and EL have to be down-selected to operate without drastic loss in performance or materials degradation. Then, we demonstrate the performance, efficiency, and durability through an accelerated stress test (AST) and daily cycling in the well-known "duck-curve" scenario which represents daily expected fluctuations in load and demands.[25]

4 Experimental

4.1 Catalyst-layer preparation

Parameters for typical catalyst ink and catalyst-layer preparation are included in Table S1. For the Pt/C inks, calculated amounts of Pt/C (45.6 wt% Pt, Tanaka), water (18.2 MΩ, Milli-Q), 1-propanol (NPA, HPLC grade, Sigma-Aldrich), and Nafion™ (5 wt% solution, 1100EW, Ion Power) are added in the stated sequence using a gravimetric method. The ink components are mixed either by manually shaking or vortexing the vial for one minute followed by sonication in a bath sonicator (M1800, Branson) equipped with a chiller (Grant) at 12°C for 30 minutes for ink volumes of <30 mL or 60 min at 10°C for ink volumes >30 mL. Similarly, for the unsupported catalyst inks, Ir-black (Tanaka) or a mixture of Ir-black and Pt-black (Tanaka), water, ethanol (200 proof, Koptec), NPA, and Nafion™ are added in the stated sequence. The vial is shaken or vortexed and then placed in an ice bath ensuring that the entire column of the ink is submersed in ice water. Using a probe tip sonicator, the tip of the probe (CPX500, Cole-Parmer) is placed 2 cm from the bottom of the vial and then the top of the vial is covered with parafilm to avoid solvent evaporation during probe sonication. Regardless of content, after sonication, the ink is immediately analyzed using dynamic light scattering (DLS, NanoPlus) (Figure S1), loaded into a syringe, and the syringe is mounted onto a spray coater for deposition.

The Nafion™ perfluorosulfonic acid membranes (N212 or N117, Ion Power) are prepared by heating in DI water at 95°C for an hour and then immersed in 0.5 M HNO_3 (ACS Reagent, Sigma-Aldrich) for an hour at room temperature to remove impurities and protonate the sulfonic-

acid groups. Finally, the treated membranes are rinsed three times with water to remove excess acid and stored in DI water until catalyst coating is performed.

For preparation of the catalyst-coated membrane (CCM), the membranes are placed on the vacuum table of the Sono-Tek Exactacoat spray coater, and sandwiched between layers of gasket materials. The membrane is allowed to dry on the vacuum hot plate at 80°C prior to deposition of the catalyst ink. The membrane is coated on both sides in order to obtain a full MEA. The atomic Ir:Pt of the catalyst layers were determined using X-ray fluorescence (Bruker, Tornado M4) (Figure S2) .

4.2 Cell Assembly

CCMs are rehydrated in room temperature water for an hour prior to cell assembly. Carbon GDLs with microporous layer (MPL) (Sigracet 29 BC) are used as FC, EL and URFC cathode GDLs. While for the EL and URFC anode titanium porous-transport layers (PTLs) (obtained from Proton OnSite/NEL) are used. The appropriate thickness PTFE (McMaster-Carr) or Tefzel™ (CS Hyde) gaskets are used in order to obtain 20% compression in GDLs, while thickness-matched gaskets are used for the Ti-PTL. For the URFC tests, the Ti-PTL was wet-proofed with PTFE dispersion (DISP 30, Ion Power) according to the procedure described by Ito et al.[26]

Two electrochemical cells are used for testing. One cell was obtained from Fuel Cell Technologies (FCT) and the other was a non-proprietary electrolysis cell provided by Proton OnSite/NEL. PTFE gaskets are used for assembly on FCT cell while Tefzel™ gaskets are used

on the NEL cell, as prescribed by the manufacturer. For FC testing, serpentine channels are used on both the cathode and anode. For EL and URFC, graphite serpentine channels are used on the HOR, HER or ORR side of the cell depending on the URFC configuration, while either parallel or serpentine channel titanium (Pt plated) flow fields are exclusively used on the OER electrode (bifunctional OER/ORR or OER/HOR). iR compensation was applied to the FC results using Ti flowfields due to a resistance that was introduced. We attributed the resistance to a contact resistance between unplated Titanium on the back side of the flowfield with the gold plated copper current collector of the cell. This resistance was not present when graphite flowfields were used.

4.3 Cell testing

A multichannel potentiostat (VSP300) from Biologic equipped with electrochemical impedance spectroscopy (EIS) and a 20A booster is used for electrochemical tests. The test station used is a modified FCT FC test stand; the modification is an addition of a water recirculation system for the EL and URFC testing. As illustrated in Figure S3, the anode side of the fuel-cell stand is modified to allow switching between gases (H_2/N_2) from the test stand and liquid water from an external diaphragm pump (KNF NF25). While 18.2 MΩ water is delivered from the temperature-regulated water reservoir, additional cell heating is provided by heating pads. For consistency between cells used and best practice for each technology, the cell temperature is controlled by a thermocouple in the endplate of the cell. In EL mode, we additionally monitor the anode outlet temperature. The temperature used throughout these studies is 80°C.

For EL-mode testing, water is recirculated on the anode side of the cell only. Conditioning consists of equilibrating the cell at 80°C for an hour with anode water flow at 100 mL min^{-1} and cathode N_2 flow at 0.17 Pa and 100% relative humidity (RH) and no back pressure. Then the cathode gas is switched to H_2 and current is stepped chronopotentiometrically (CP). The CP steps are evenly spread from 0.01 A/cm^2 to 2 A/cm^2 with durations of 2 min $step^{-1}$ for all steps except 2 A cm^{-2}, which has duration of 2 hr. After 2 h at 2 A cm^{-2}, the rest of the CP steps are performed in reverse order. Average voltage values for the t = 110-120 s are used for each step.

The FC is conditioned by running 16 to 20 h chronoamperometry (CA) at 600 mV applied potential (vs anode) with the cell at 80°C, H_2 on anode at 0.42 Pa and 100% RH, air on cathode at 0.84 Pa and 100% RH, and no back pressure on either cathode or anode. A successful break in of the cell is signified by a several hour plateau in the CA curve at a significantly increased current density than that recorded during the initial few hours. The flow rates on cathode and anode are then increased to 1.52 Pa Air or O_2 and 0.76 Pa H_2, respectively, and the back pressures on both electrodes are set at 145 kPa prior to generating FC polarization curves. Screening FC performance is first assessed via cyclic voltammetry (CV) from 200 to 950 mV vs anode at 20 mVs^{-1}, and then by collecting CA currents for 2 minutes at 100 mV potential steps from 200 to 950 mV. The upper limit of the potential window is selected to be 30 to 40 mV lower than the open-circuit voltage (OCV) for each cell and is adjusted accordingly.

The URFC measurements are initiated with FC conditioning protocol and FC measurements are performed first followed by EL without additional conditioning in EL mode. When switching

modes, both cathode and anode are purged with N_2 at 0.84 Pa for 15 min prior to flowing appropriate gases or water and performing electrochemical measurements.

ASTs are performed on the final down-selected URFC MEA and cell. The protocol is chosen by combining the currently-available FC and EL ASTs.[27, 28] A triangle-wave cycling profile is applied to the anode side of the cell, biased against the cathode counter electrode/reference electrode, the voltage profile is 0.05 to 1.55 V or 0.55 to 1.55 V, for typical voltage ranges of CE and CG URFC cycles, respectively as shown in SI Figure S4. The potentials for ASTs are chosen to reflect the potential window the Ir-black+Pt-black electrode would be exposed to as the URFC undergoes the complete charge (EL) and discharge (FC) operation in CE and CG configurations. Thus, we are mainly probing the voltage effects on degradation of the CE-URFC MEA. The cycle is repeated 10,000 times at a rate of 300 mV/sec. At regular and convenient (manual operation and overnight test) intervals, the cycle is stopped and FC and EL performance tests are performed under the standard conditions described above to ascertain the change in performance as a result of the AST cycles. We emphasize that under both CE and CG ASTs, the performance of the MEA is always tested in CE mode for consistency. Aliquots of the water are then collected for dissolved ions analysis from AST and charge-discharge cycling. The water samples were quantified by inductively coupled plasma mass spectroscopy (7900 ICP−MS, Agilent) using the He mode. The internal standard was Bi selected based on its first ionization potential and M/Z as compared to Ir and Pt. As a final demonstration, a duck-curve profile where the URFC cell is charged for 6 h and discharged for 4 h. During durability testing, the URFC cell is held either at ±1 A/cm^2 using CA.

For all efficiency calculations we follow the guidance from Harrison et al. and detailed in SI, the thermodynamic values have been adjusted for temperature (80 °C) and pressure (145 kPa).[29] We note that since the EL efficiencies are calculated based on the enthalpy of hydrogen (at reaction temperature and pressure) and required heat input corresponding to 1.42 V, divided by the URFC operating cell voltage at desired charging current. Nonsense efficiencies higher than 100% are possible at low current densities since the heat input is not included, while being provided by the resistive losses of the cell.

4.4 Techno-economic analysis

We adopt the levelized cost of storage metric (LCOS) of Schmidt et al. 2018,[5] and use the approach for techno-economic analysis described in Wei et al 2014 and Scataglini & Wei 2017 that includes bottom-up cost analysis of the URFC or RFC cell stack(s), development of system schematic design and identification of balance of plant (BOP) components, and BOP component cost estimation.[30, 31] For all cost calculations, a 250 kW system is used.

5 Results and Discussion

The MEA design philosophy consisted of optimizing the FC and EL discreetly, meaning using cells, diffusion media, and membranes optimized for the separate cells. The results from discrete systems are used to understand the origin of the losses as we compromise upon combining the components into a URFC MEA, cell, and diffusion media. The membrane, catalyst and diffusion media chosen are commercially-available materials used to obtain a baseline performance and a degree of robustness for the work. To avoid carbon corrosion, Pt/C catalysts, carbon GDLs and graphite flow-fields are not used above 1 V. Instead, Ti-PTL, Ti flow-fields and unsupported Pt-

black and Ir-black are used for electrodes experiencing potentials above 1 V. Aside from the choice of catalyst, the membrane is the second critical component that can drastically contribute to decreased voltage efficiency.[32] Membranes are pretreated by boiling in order to obtain the highest conductivity, to reduce in-cell swelling, and to stabilize the membranes for operation under liquid operation (EL mode). While state-of-the-art (SOA) FC membranes are very thin, i.e. less than 10 μm, we use N212 (51 μm) as it is still the most commonly used research FC membrane, and ideal for comparison to literature results.[33, 34] Similarly, for EL tests, N117 (183 μm) is used as it represents a SOA membrane and a direct comparison to literature results.[35] Thus for URFC testing, we chose to use N212 as a compromise membrane since the purpose of this investigation is to identify a competitive configuration for a URFC, and demonstrate it in terms of upper limit of RTE. We point out here that the final choice of membrane will ultimately depend on the system design parameters and whether to include electrochemical compression of H_2 and perhaps O_2 as well. It should also be noted that oxygen storage is deemed optional depending on technology and usage. An O_2 cathode feed can generate higher power output than air where it is necessary. Depending on the system choice, the ultimate operation may require differential or balanced pressure, in which case gas crossover must be taken into account and mitigated. Mitigation in electrolysis is typically achieved by increasing the membrane thickness and through the use of other crossover mitigation strategies,[36] and is beyond the scope of this paper.

The electrolysis optimization is performed on N117, keeping the EL cathode catalyst loading constant at 0.3 mg/cm^2 Pt (from Pt/C). It has previously been demonstrated by Bernt and Gasteiger that 11.6 wt% ionomer content (with respect to catalyst weight) generates the best

activity when titanium dioxide-supported iridium oxide (Umicore) is the anode catalyst.[37] Our investigations (Figure S5) also confirm a similar trend when Ir-black is used as the anode catalyst. For the URFC anodes, the Ir-black to Pt-black atomic ratio is varied at a fixed total platinum group metal (PGM) loading of 1 mg/cm^2 while keeping the ionomer content at 11.6 wt%. The resulting electrolyzer polarization curves are presented in Figure 3. The performances are also compared to a baseline EL MEA containing only Ir-black on the EL-anode. From the polarization curves in Figure 3, it is apparent that the substitution of the stated fraction of Ir-black in the anode catalyst layer with Pt-black leads to, as expected, an almost linear loss in its oxygen evolution performance. Increasing the Pt loading in the EL-anode catalyst layer results in at least 40 mV penalty at 1 A/cm^2 when 10 at% Pt is substituted for Ir as compared to the baseline's performance. When Pt content is increased further it results in higher losses, especially at higher current densities. Here, the potential advantage of the CE configuration is evident in that only a small amount of Pt-black is expected to be sufficient since the anode is catalyzing hydrogen oxidation, a relatively facile electrochemical reaction, in FC mode. While in CG configuration, the kinetically sluggish ORR will need a higher amount of Pt, resulting in lower EL performance.

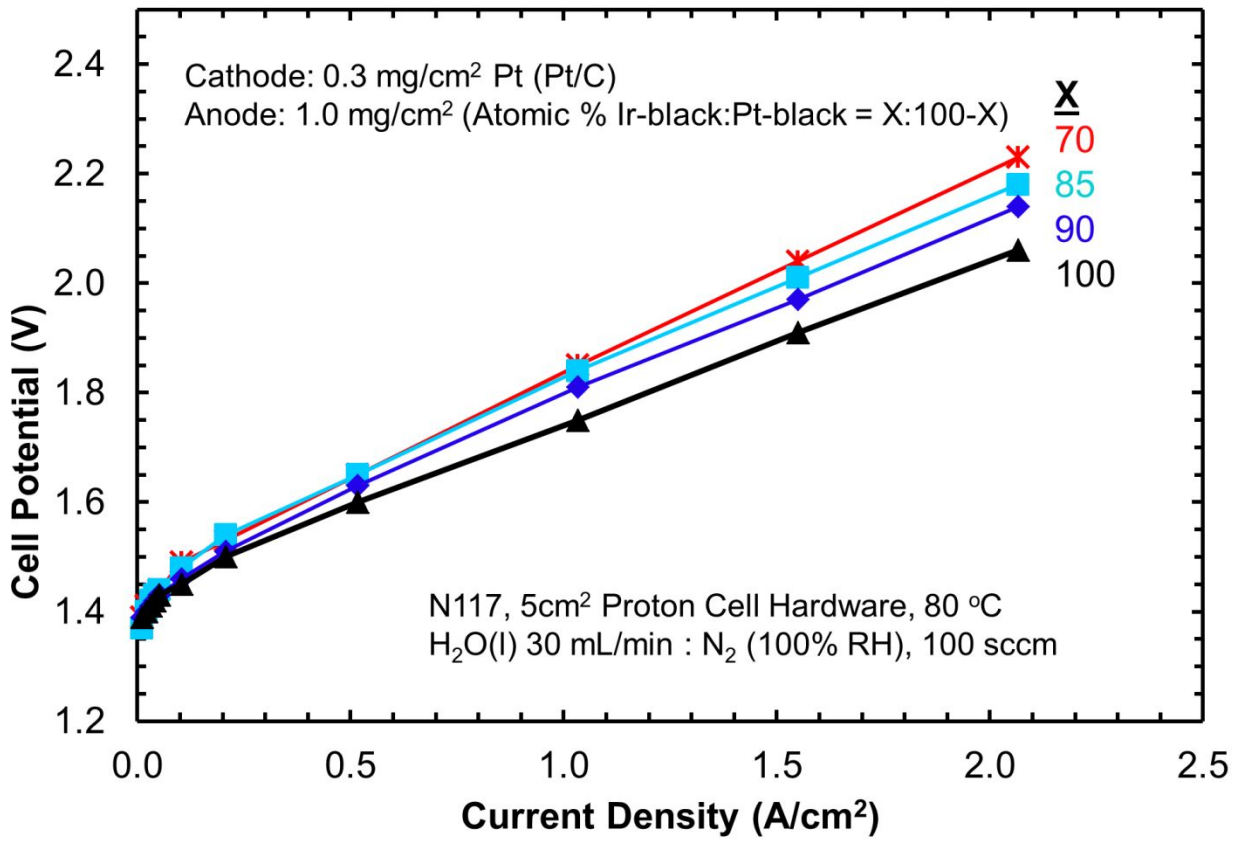

Figure 3. Polarization curves for discrete electrolyzers using N117 with various Ir-black (X, balanced by Pt-black) ratios on the anode. The activities are not iR corrected. Anode side contains 25 cm² parallel titanium flow field reduced to 5 cm² with gaskets and Ti PTL. Cathode side contains 25 cm² single serpentine graphite flow field, reduced to 5 cm² with gaskets, and 29 BC GDL.

For FC optimization, CCMs are prepared on N212 with the FC-cathode catalyst loading of 0.3 mg/cm² Pt (from Pt/C), while the FC-anode Ir-black to Pt-black atomic ratio was varied, at a fixed total PGM loading of 1 mg/cm². The resulting FC performances are presented in Figure 4, and compared to a baseline FC MEA containing only Pt/C (0.3 mg/cm² Pt) as the FC-anode. Contrary to expectations, an increase in Pt-black content in the anode did not lead to improvements in FC performance. While an anode with 10 at% Pt-black (X = 90) performs statistically similar to the baseline (100 at% or 0.3 mg/cm² Pt from Pt/C), a subsequent increase in Pt-black content leads to a decrease in FC performance for 85 at% and 70 at%. Since

geometric HOR active site density is much higher than at 90 at% Ir, one can speculate that the performance losses are either due to ohmic or mass-transport limitations on the URFC anodes at higher Pt content. However, increase in metallic Pt content in the catalyst layer should lead to improved conductivity rather than increased ohmic losses since the I:C ratio and catalyst layer thickness is uniform across the MEAs. Thus, a mass-transport limitation is a more probable cause. The FC with a 90 at% Ir-black (10 at% Pt-black) anode generates 0.71 V at 1 A/cm^2, which is marginally higher than the 0.70 V generated by the baseline FC. Anode Pt loadings lower than 10 at% Pt-black also lead to substantial loss in cell voltage. In order to further investigate the unexpected results with increasing Pt black loading in the bifunctional electrodes, we prepared FC MEAs with varying loadings of Pt-black catalyst on one half of the MEA, and tested that electrode as an anode (HOR) or cathode (ORR). The unexpected results shown in Figure S are in alignment with Figure 4, in which the performance of Pt black in either HOR or ORR shows a non-linear dependence on loading, with 0.3 mg/cm^2 being best, while HOR performs significantly better than ORR. Further investigations are underway to understand the unexpected trend observed for Pt and Ir-black mixed electrodes at higher Pt-black contents.

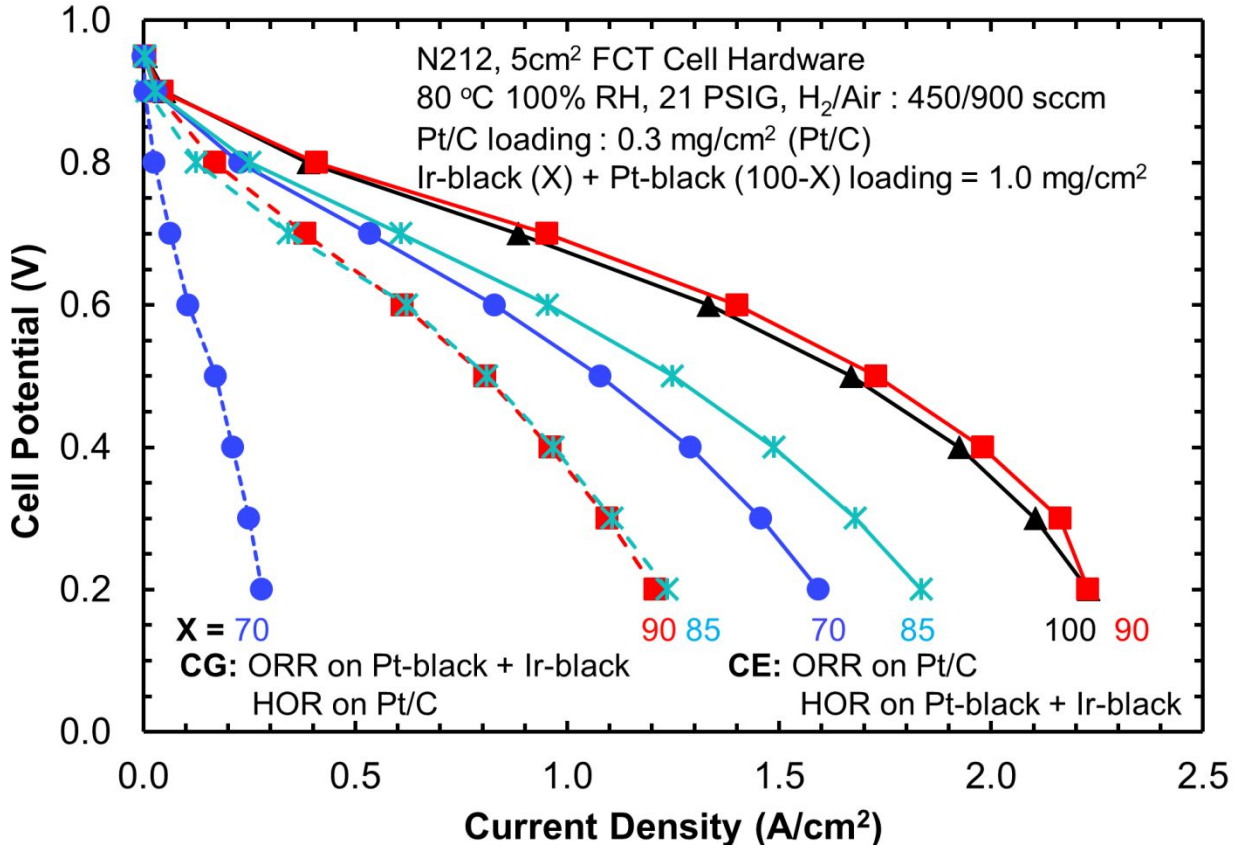

Figure 4. Polarization curves for discrete fuel cells on N212 with various Ir-black (balanced by Pt-black) ratios on the bifunctional electrode. Solid lines represent CE configuration, while dashed lines represent CG configuration testing of the bifunctional electrode. The activities are not iR corrected. Both cathode and anode comprise of 5 cm² single serpentine graphite flow fields and 29 BC GDLs. Black curve represents baseline with 0.3 mg/cm² Pt loading from Pt/C on both cathode and anode.

As a comparison to the traditional CG-configuration URFC cell, we also show in Figure 4, the corresponding performance of the Pt- and Ir-black cathodes (used as ORR electrode). First, it is clear that the CG-configuration URFC cannot obtain comparable performance to the CE-configuration, at least when unsupported Pt catalyst is used, even with optimized GDLs and flow fields for ORR. Switching to Ti PTL instead of 29 BC and Ti parallel flow field instead of serpentine graphitic for URFC incur additional performance losses (Figure S7). Secondly, the higher Pt loading required for the ORR is also bound to result in reduced performance in EL

mode, as is apparent from Figure 3. Thus, even before the diffusion media and flow fields are compromised, the CG configuration suffers an operating penalty of 300 mV at 1 A/cm^2 for a 90 at% Ir-black cathode. The 90 at%- 10 at% Ir-black and Pt-black composite catalyst layer is selected as the optimal electrode for CE-URFC operation.

Next we assess the RTE of optimized URFC MEAs, in URFC cell hardware. The URFC catalyst layers are evaluated on the same N212 (51 μm) membrane instead of thicker N117 (183 μm) used for the discrete EL. As shown in Figure 5, using N212 as the membrane and employing the URFC MEA as FC and EL improves the RTE to 57% at 1 A/cm^2 and 30% at 2 A/cm^2 (Table S2). As shown by the overlaid efficiency curve, the URFC can achieve higher RTE if operated at lower current densities. For comparison, Figure S8, shows the comparable RTE for a discrete RFC system. In the discrete configuration, the optimal EL and FC have efficiencies of 81% and 58%, respectively at 1 A/cm^2, corresponding to 47% RTE for the URFC. Thus, using the CE configuration, minimal compromise in performance or efficiency is made with appropriate adjustments of components, as demonstrated here by using N212 instead of N117 membrane. More importantly, for the balance of stack cost, membrane cost is decreased by 50% (one membrane for URFC vs two for discrete system), Pt content by 55% (0.4 mg/cm^2 total platinum loading in URFC vs 0.9 mg/cm^2 in discrete), and 10% reduction for Ir content (1.0 mg/cm^2 for discrete vs 0.9 mg/cm^2 for URFC). Thus, there are distinct advantages for reducing the capex and opex, depending on the ultimate in cell pressurization chosen.

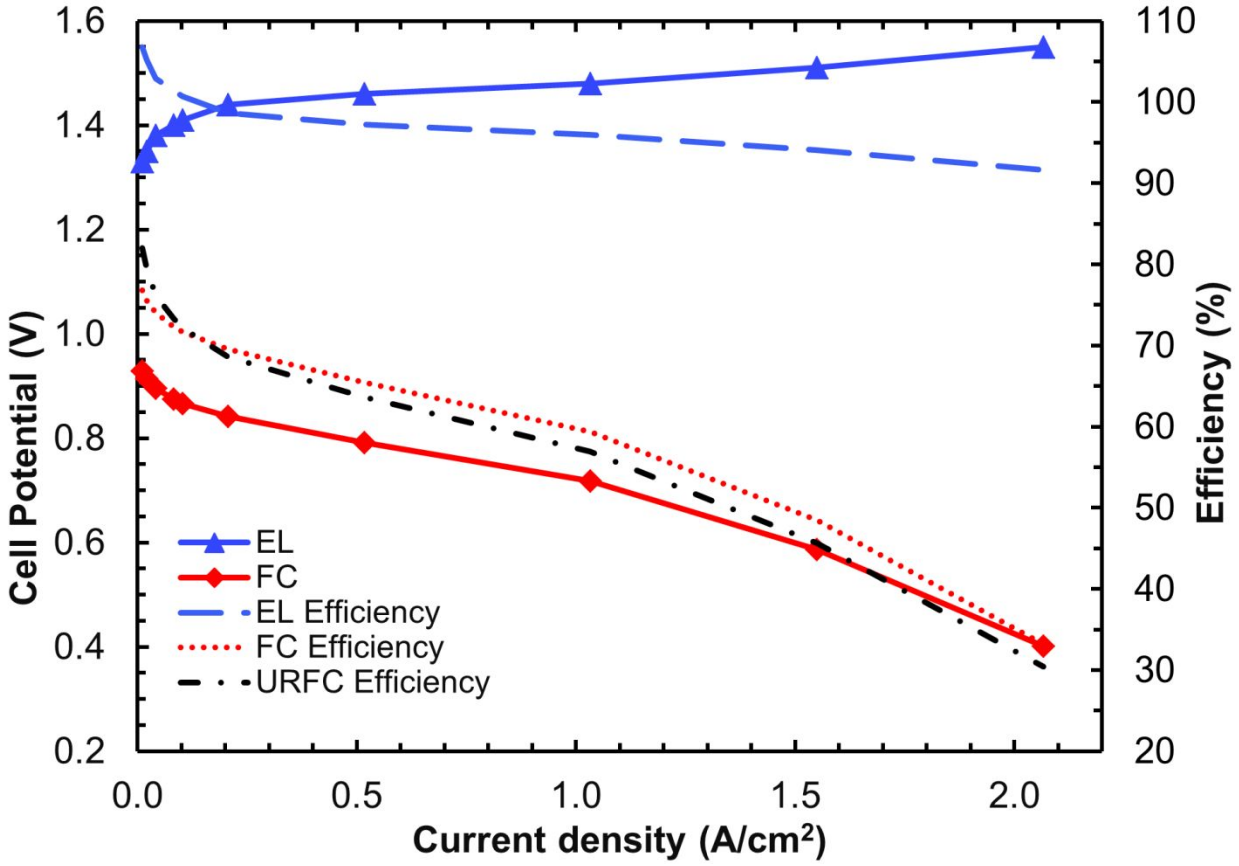

Figure 5. Polarization curves for a unitized regenerative fuel cell using N212 with the optimal 90 at% Ir-black (10 at% Pt-black) in the anode catalyst layer. FC performance is obtained using air as reactant. FC and EL polarization curves (solids) were obtained using the same MEA, same FCT cell hardware with titanium triple serpentine flowfield and titanium PTL loaded with 3 wt% PTFE on anode, and triple serpentine graphite flowfield and 29 BC GDL on cathode. FC, EL, and URFC efficiencies are plotted on the secondary y-axis. The FC activities are iR corrected for resistance associated with titanium flowfield.

To determine the highest RTE achievable with the URFC hardware, FC polarization curves were acquired for the URFC MEA using O_2 as the cathode gas rather than air (Table S2). As shown in Figure S9, FC performance in the kinetic region is identical when using O_2 or air on the cathode. As expected, the onset of the mass-transport-limited region is at much lower current densities for air feed on cathode than for O_2 feed. As apparent from Figure 6, even with the use of titanium flowfield and PTL on the anode, RTE efficiencies are improved, resulting in RTEs of 61% and 50%, at 1 and 2 A/cm^2, respectively. The losses resulting from hardware compromises (Figure

S7) are easily compensated by adjustments in cathode feed. This RTE is the highest reported to date for any low temperature URFC system (Table S3),[13, 38] bettered only by solid oxide fuel cells (SOFCs) operating at much higher temperatures.[39, 40] Duan et al. recently reported a protonic ceramic URFC which achieved 75% RTE at 840 mA/cm^2 in charge and 140 mA/cm^2 in discharge mode.[39] The RTE for the URFC in Figure 6 at those charge-discharge values is 70%. Although the SOFC reported a higher RTE, they however suffer from the need to ramp up to higher temperatures during start-up and cannot idle. Additionally, operational and manufacturing costs are also higher for SOFCs due to the need to manage heat and the need to use thermally stable components at elevated temperatures.

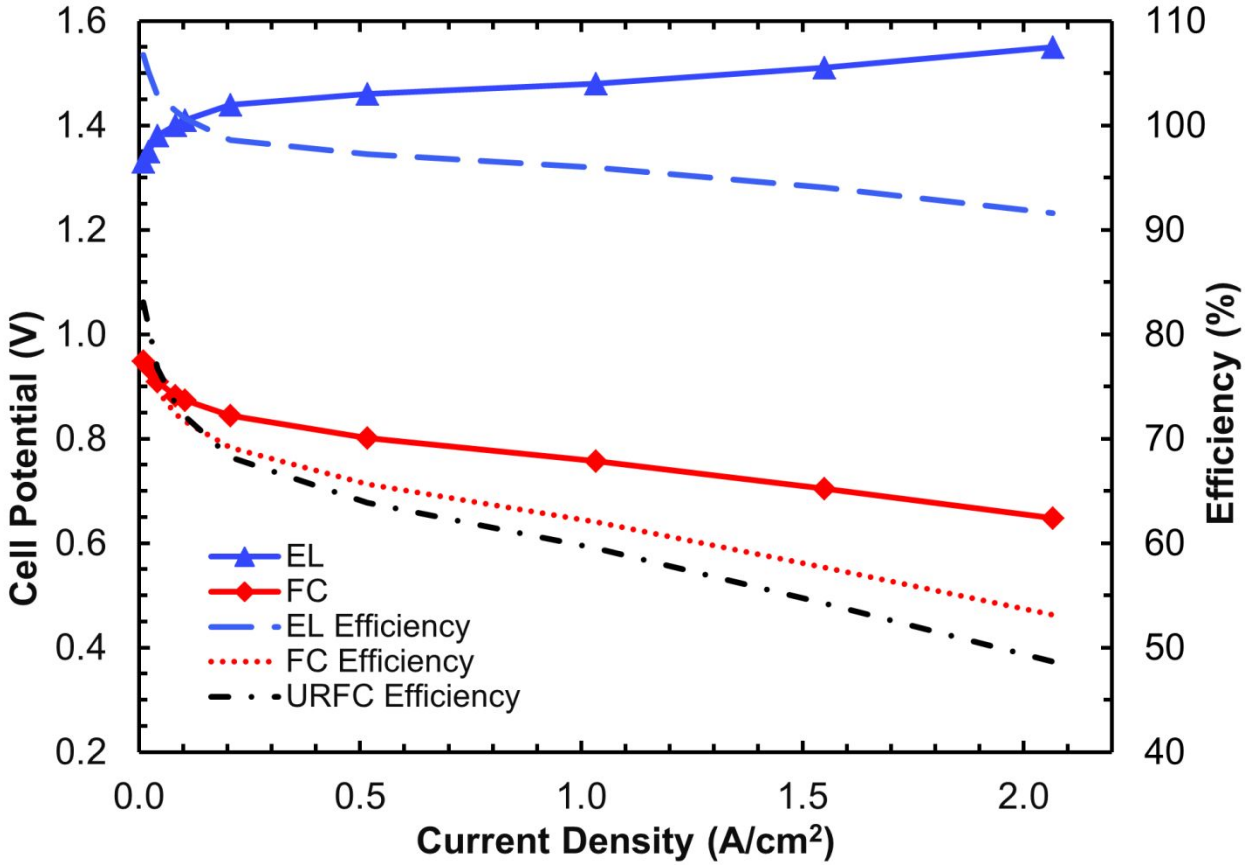

Figure 6. Polarization curves for a unitized regenerative fuel cell using N212 with the optimal 90 at% Ir-black (10 at% Pt-black) in the anode catalyst layer. FC performance is obtained using O_2

as reactant. FC and EL polarization curves (solids) were obtained using the same MEA, same FCT cell hardware with titanium triple serpentine flowfield and titanium PTL loaded with 3 wt% PTFE on anode, and triple serpentine graphite flowfield and 29 BC GDL on cathode. FC, EL, and URFC efficiencies are plotted on the secondary y-axis. The FC activities are iR corrected for resistance associated with titanium flowfield.

To assess the durability of the optimized URFC MEA and cell, voltage-cycling ASTs are performed to accelerate catalyst degradation.[41-43] First, a FC break-in is performed, followed by the beginning of life (BOL) performance assessment in FC mode. Transitions are handled by switching anode to liquid water flow and cathode to nitrogen, followed by BOL performance in EL mode. The AST cycling is then initiated, consisting of cyclic anode voltage from 1.55 V to 0.05 V (CE mode) or 0.55 V (CG mode). These voltage windows correspond to the expected voltages the anode electrode would experience in FC and EL operation at 1 A/cm^2 (Figure 6). After a certain number of AST cycles, the cycling is stopped to allow for FC and EL performances to be recorded prior to resuming the AST. We note that any performance loss could arise from a combination of degradation of both electrodes, membrane, or wetting of the GDL/PTL. The voltage efficiency is assessed from the EL or FC voltages at cycle "n" divided by the BOL cell voltage and plotted in Figure 7. The results show that in CE and CG configuration, the EL and FC voltage efficiency and RTEs are maintained for several thousand cycles. The EL performance is maintained at almost 100% for the entire duration of 10k cycles, while the FC performance starts degrading between 2k and 7k cycles. Prior to degradation however, the FC performance actually improves, i.e. the potential at 1 A/cm^2 load increases from 0.69 V to 0.73 V. The observations are similar to previous FC break in protocols where hydration of the membrane shows apparent improvement in activity.[44] Most of the BOL efficiency penalties shown in Figure 7, when compared to Figure 5, can be attributed to the use of parallel flowfields

and Ti-PTL on the anode side (Figure S7). This could easily be compensated by using O_2 instead of air as the cathode feed, as demonstrated in Figure 6.

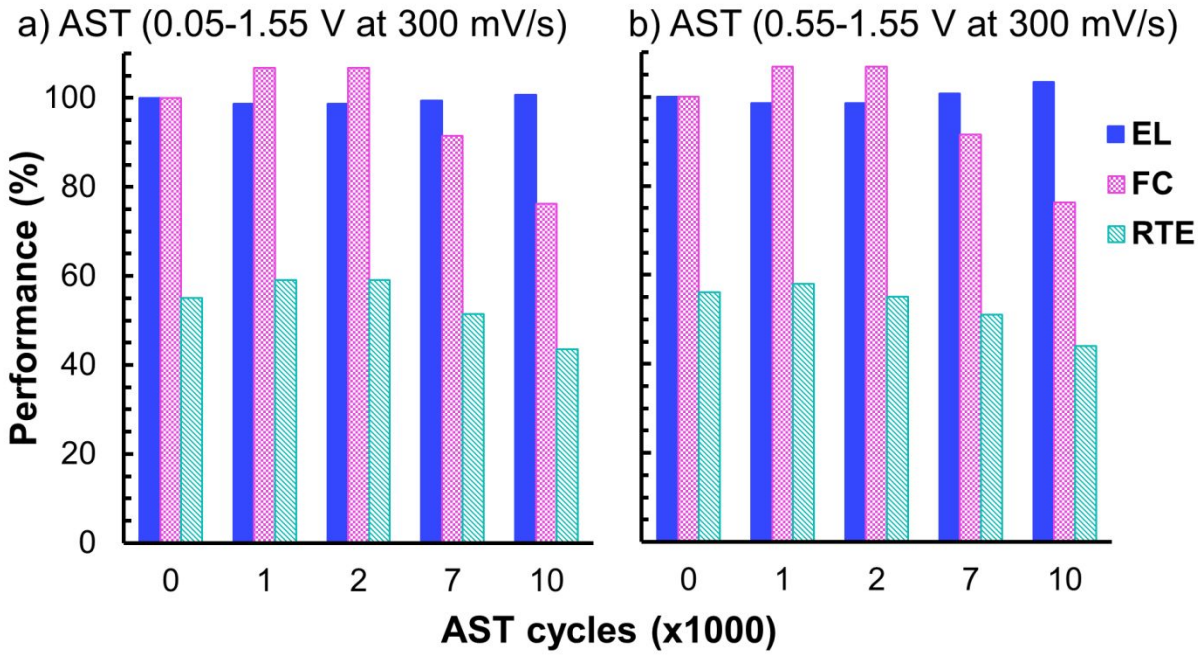

Figure 7. Demonstration of a 5 cm² URFC MEA under AST cycling durability tests in potential window corresponding to (a) CE configuration and (b) CG configuration. Performances are evaluated in CE configuration irrespective of the AST potential window. For simplicity "Performances" represent two things. For EL, FC they are defined as voltage efficiency, calculated from the cell potential required to generate 1 A/cm² during AST cycle "n" divided by the BOL cell potential. While for RTE, they are the corresponding RTE at cycle "n".

Comparing the CG and CE AST cycling on the URFC anode in Figure 7, shows that the stability over the lifetime of the URFC is similar although the potential cycling window (Figure S4) for the CG configuration is narrower (0.55-1.55 V) than for the CE configuration (0.05-1.55 V). The same initial improvement in FC activity is seen in the CG cycling window, before degrading beyond 2k AST cycles. This is a reassuring result, since one of the potential disadvantages of the CE configuration is that the lower potentials required for HOR on the anode (versus ORR on the cathode) will lead to faster degradation of the anode catalyst layer compared to the oxygen

electrode in the CG configuration. Results in Figure 7 are also consistent with previous observations since the differential potential window (0.05-0.55 V) for the electrode between CG and CE configurations is below the potential threshold for voltage dependent Pt-dissolution.[45] Most importantly, the RTE after 10k cycles is better than all BOL RTEs reported thus far at 1 A/cm^2 for PEM based URFCs (see Table S3).[13, 38]

We also demonstrate the application of the CE-URFC in a duck-curve energy-storage scenario in which the cell is charged at 1A/cm^2 for 6 h, followed by discharging at 1A/cm^2 for 4 h (Figure 8). One day's worth of stable charge and discharge, with an average RTE of 54% are shown in Figure 8, operating on air during discharge. Neither the AST cycling tests nor the charge-discharge cycling showed detectable amount of Ir and Pt dissolution using ICP-MS analysis (Table S4). Although Pt and Ir could migrate into the membrane and ionomer phase in the catalyst layers, this was outside the scope of our current work.

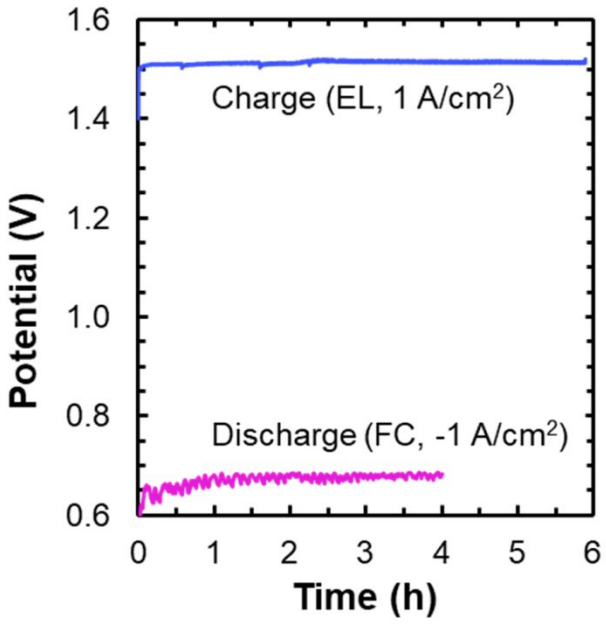

Figure 8. Demonstration of a 5 cm² URFC MEA operating in a duck-curve duty cycle in CE configuration with a balanced 1 A/cm² charge and subsequent discharge (air).

Finally, we performed a preliminary cost analysis (Table 1) comparing CE and CG configuration. As a comparison, we have also included analysis for a discrete RFC with N212 membrane for both EL and FC mode.

Table 1. Cost comparison for CE and CG URFC with discrete RFC.

Case	**a-CE**	**b-CG**	**c-CG**	**d-RFC**
System capital cost ($/kW)	1464	1413	1470	1870
H_2 storage cost ($/kWh)	18	18	18	18
Total PGM (mg/cm²)	1.3	1.3	2.0	0.6(FC), 1.3(EL)
N_2 gas cost ($/yr)	3500	0	0	0
RTE (%)	57	33	50	57

FC efficiency (%)	58	33	51	58
EL efficiency (%)	99	99	99	99
Lifetime (yr)	15	15	15	15
LCOS ($/kWh)	0.308	0.358	0.312	0.357

We assume for the purposes of this work that (1) the stack and system lifetimes are equivalent for both configurations (Figure 7); (2) that the key difference in the balance of plant components for the CE configuration is the inclusion of an N_2 purge subsystem that is required when switching between operation modes; (3) a daily duty cycle of 6 hours charging followed by 4 hours discharging (Figure 8); and (4) future capital costs corresponding to much higher PEM industry production volumes. With these assumptions, we estimate about a 5% increase in the BOP cost and about $3500/year N_2 gas cost for the CE case. Assuming the same PGM loading for the two cases, the FC and RTE of the CE configuration is much higher than the CG configuration (Case a vs Case b in Table 1 above). The higher RTE is more than sufficient to offset the slightly higher URFC capital and operating cost from N_2-purge in the CE configuration. The LCOS of case a is about 14% lower than LCOS of case b. We also consider the case of higher PGM loading in the CG configuration to improve the FC mode efficiency. In this case, the URFC capital cost is slightly higher than the CE case but the LCOS for the CE case is still slightly lower (case a vs case c). The LCOS for the CE configuration (case a) is also seen to be about 14% lower than the reference discrete RFC (case d), i.e. a system with a discrete EL and discrete FC. The URFC configurations in Table 1 have about 22% lower system capital cost driven largely from the cost reduction derived from consolidation of the stacks.

6 Conclusions

We have demonstrated operating round trip efficiencies (RTEs) of a unitized regenerative fuel cells (URFCs) in the two possible configurations. From the discussions and results presented here, it can be concluded that URFCs in constant-electrode (CE) configuration where all reductions (HER/ORR) take place on cathode and all oxidations (HOR/OER) on anode can achieve RTEs of 60% (at 1 A/cm^2), comparable to discrete fuel cells and electrolyzers. URFCs operating in CE configuration perform significantly better than in constant-gas (CG) configuration where the oxygen reactions (ORR/OER) take place on one electrode and the hydrogen reactions (HOR/HER) take place on the other. Compared to discrete mode, URFCs achieve significant catalyst (10% Ir and 55% Pt) and membrane (50%) reductions, in addition to simplifying or reducing balance-of-plant components. Our initial assessment of various compromises and configurational modifications necessary to translate a PEM-based electrolyzer (EL) and fuel cell (FC) into a unitized system shows that penalties incurred can mostly be overcome or minimized by operating in CE configuration. We demonstrate that a 10 at% Pt-black/90 at% Ir-black bifunctional HOR/OER anode catalyst layer is sufficient to maintain HOR activity in FC comparable to a baseline FC, while the higher Ir-black loadings incur a minimal performance loss in EL mode. This high efficiency can largely be maintained over 10k accelerated stress test (AST) cycles. We also demonstrate the CE-URFC in a duck curve reflecting daily fluctuations in energy load and demand, energy-storage scenario by charging for 6 h, and discharging for 4 h. Finally, preliminary cost analysis of the two configurations show that URFC operation in CE configuration has the potential to reduce cost of energy storage compared to the traditional CG case, resulting a levelized cost of energy storage of 0.308$/kWh well within the range of competing technologies. The URFC capital cost is about 22% lower than

using discrete EL and FC units to form regenerative fuel cell (RFC) system. Levelized cost of CE URFC is 14% lower than the RFC. Although CG-configuration URFCs have been investigated, and to a limited extent even employed, CE-configuration URFCs hold promise as a technology that is ready for systems integration. Our assessments suggest that the primary challenge to CE-configuration URFCs will be to engineer catalyst layers and systems that are stable in both charge (EL) and discharge (FC) operating modes. However, with copious amount of technology readily available for improvements in terms of materials and system configurations, there is ample promise for further progress and wider implementation of URFCs.

7 Acknowledgements

The authors acknowledge the Department of Energy – Office of Energy Efficiency and Renewable Energy - Fuel Cell Technologies Office (DOE-EERE-FCTO) and program managers Greg Kleen and Dimitrios Papageorgopoulos for funding under Contract Number DE-AC02-05CH11231. The submitted manuscript was created, in part, by U Chicago Argonne, LLC, Operator of Argonne National Laboratory, Argonne, U.S. Department of Energy Office of Science laboratory, operated under Contract No. DE-AC02-06CH11357. The authors thank: Alexy Serov, Chris Capuano, K.C. Neyerlin, Jacob Spendelow, Rangachary Mukundan, and Shaun Alia for insightful discussions as part of the Regenerative Fuel Cell Working Group. We thank Guiji Liu and Francesca Toma for access to ICP-MS. We also thank Proton OnSite/NEL for Ti PTLs. ND, AW and DM conceived the project and secured funding; ND, YR, JF, MW and XP designed and conducted the experiments; YR, JF, MW and ND composed the manuscript, and all the authors edited the written work.

8 References

1. T. M. Gür, *Energy Environ. Sci.*, 2018, **11**, 2696-2767.
2. J. Schmidt, K. Gruber, M. Klingler, C. Klöckl, L. Ramirez Camargo, P. Regner, O. Turkovska, S. Wehrle and E. Wetterlund, *Energy Environ. Sci.*, 2019, **12**, 2022-2029.
3. O. Krishan and S. Suhag, *Int. J. Energy Res.*, 2019, **43**, 6171-6210.
4. S. J. Davis, N. S. Lewis, M. Shaner, S. Aggarwal, D. Arent, I. L. Azevedo, S. M. Benson, T. Bradley, J. Brouwer, Y. M. Chiang, C. T. M. Clack, A. Cohen, S. Doig, J. Edmonds, P. Fennell, C. B. Field, B. Hannegan, B. M. Hodge, M. I. Hoffert, E. Ingersoll, P. Jaramillo, K. S. Lackner, K. J. Mach, M. Mastrandrea, J. Ogden, P. F. Peterson, D. L. Sanchez, D. Sperling, J. Stagner, J. E. Trancik, C. J. Yang and K. Caldeira, *Science*, 2018, **360**.
5. O. Schmidt, S. Melchior, A. Hawkes and I. Staffell, *Joule*, 2019, **3**, 81-100.
6. A. R. Dehghani-Sanij, E. Tharumalingam, M. B. Dusseault and R. Fraser, *Renew. Sustain. Energy Rev.*, 2019, **104**, 192-208.
7. B. Pivovar, N. Rustagi and S. Satyapal, *Interface*, 2018, **27**, 47-52.
8. F. Mitlitsky, B. Myers and A. H. Weisberg, *Energy Fuels*, 1998, **12**, 56-71.
9. A. Kusoglu and A. Z. Weber, *Chem. Rev.*, 2017, **117**, 987-1104.
10. R. Baldwin, M. Pham, A. Leonida, J. McElroy and T. Nalette, *J. Power Sources*, 1990, **29**, 399-412.
11. J. Ahn and R. Holze, *J. Appl. Electrochem.*, 1992, **22**, 1167-1174.
12. B. Paul and J. Andrews, *Renew. Sustain. Energy Rev.*, 2017, **79**, 585-599.
13. Y. Wang, D. Y. C. Leung, J. Xuan and H. Wang, *Renew. Sustain. Energy Rev.*, 2016, **65**, 961-977.
14. S. A. Grigoriev, P. Millet, V. I. Porembsky and V. N. Fateev, *Int. J. Hydrogen Energy*, 2011, **36**, 4164-4168.
15. T. Sadhasivam, K. Dhanabalan, S.-H. Roh, T.-H. Kim, K.-W. Park, S. Jung, M. D. Kurkuri and H.-Y. Jung, *Int. J. Hydrogen Energy*, 2017, **42**, 4415-4433.
16. M. Gabbasa, K. Sopian, A. Fudholi and N. Asim, *Int. J. Hydrogen Energy*, 2014, **39**, 17765-17778.
17. H. Ito, N. Miyazaki, M. Ishida and A. Nakano, *Int. J. Hydrogen Energy*, 2016, **41**, 5803-5815.
18. P. Millet, R. Ngameni, S. A. Grigoriev and V. N. Fateev, *Int. J. Hydrogen Energy*, 2011, **36**, 4156-4163.
19. G. C. da Silva, K. J. J. Mayrhofer, E. A. Ticianelli and S. Cherevko, *J. Electrochem. Soc.*, 2018, **165**, F1376-F1384.
20. T. Sadhasivam, G. Palanisamy, S.-H. Roh, M. D. Kurkuri, S. C. Kim and H.-Y. Jung, *Int. J. Hydrogen Energy*, 2018, **43**, 18169-18184.
21. S. A. Grigoriev, P. Millet, K. A. Dzhus, H. Middleton, T. O. Saetre and V. N. Fateev, *Int. J. Hydrogen Energy*, 2010, **35**, 5070-5076.
22. G. Chen, S. R. Bare and T. E. Mallouk, *J. Electrochem. Soc.*, 2002, **149**.
23. Y.-J. Wang, B. Fang, X. Wang, A. Ignaszak, Y. Liu, A. Li, L. Zhang and J. Zhang, *Prog. Mater Sci.*, 2018, **98**, 108-167.
24. R. Omrani and B. Shabani, *Int. J. Hydrogen Energy*, 2019, **44**, 3834-3860.

25. P. Denholm, M. O'Connell, G. Brinkman, J. Jorgenson *Overgeneration from Solar Energy in California – A Field Guide to the Duck Chart*, Department of Energy's (DOE) Office of Energy Efficiency and Renewable Energy (EERE), 2015.
26. H. Ito, K. Abe, M. Ishida, C. M. Hwang and A. Nakano, *Int. J. Hydrogen Energy*, 2015, **40**, 16556-16565.
27. S. M. Alia and G. C. Anderson, *J. Electrochem. Soc.*, 2019, **166**, F282-F294.
28. C. Rakousky, U. Reimer, K. Wippermann, S. Kuhri, M. Carmo, W. Lueke and D. Stolten, *J. Power Sources*, 2017, **342**, 38-47.
29. K.W. Harrison, R. Remick, and G.D. Martin, Hydrogen Production: Fundamentals and Cas Study Summaries, Essen, Germany, 05/21/2010, 2010.
30. M. Wei, T. Lipman, A. Mayyas, J. Chien, S. H. Chan, D. Gosselin, H. Breunig, M. Stadler, T. McKone, P. Beattie, P. Chong, W. G. Colella, B. D. James, *A Total Cost of Ownership Model for Low Temperature PEM Fuel Cells in Combined Heat and Power and Backup Power Applications* Lawrence Berkeley National Laboratory, Berkeley. CA, 2014.
31. R. Scataglini, M. Wei, A. Mayyas, S. H. Chan, T. Lipman and M. Santarelli, *Fuel Cells*, 2017, **17**, 825-842.
32. A. L. Vielstich, H. A. Gasteiger, *Handbook of Fuel Cells: Fundamentals, Technology, Applications*, John Wiley and Sons Ltd, Chichester, England, 2003.
33. K. M. Rod Borup, Adam Weber, *Fuel Cell Performance and Durability Consortium*, United States Department of Energy Fuel Cell Technology Office, Washington DC, 2018.
34. T. Yoshida and K. Kojima, *Interface*, 2015, **24**, 45-49.
35. G. Bender, M. Carmo, T. Smolinka, A. Gago, N. Danilovic, M. Mueller, F. Ganci, A. Fallisch, P. Lettenmeier, K. A. Friedrich, K. Ayers, B. Pivovar, J. Mergel and D. Stolten, *Int. J. Hydrogen Energy*, 2019, **44**, 9174-9187.
36. P. Trinke, P. Haug, J. Brauns, B. Bensmann, R. Hanke-Rauschenbach and T. Turek, *J. Electrochem. Soc.*, 2018, **165**, F502-F513.
37. M. Bernt and H. A. Gasteiger, *J. Electrochem. Soc.*, 2016, **163**, F3179-F3189.
38. M. Hunsom, D. Kaewsai and A. M. Kannan, *Int. J. Hydrogen Energy*, 2018, **43**, 21478-21501.
39. C. C. Duan, R. Kee, H. Y. Zhu, N. Sullivan, L. Z. Zhu, L. Z. Bian, D. Jennings and R. O'Hayre, *Nat. Energy*, 2019, **4**, 230-240.
40. S. Choi, T. C. Davenport and S. M. Haile, *Energy Environ. Sci.*, 2019, **12**, 206-215.
41. O. Kasian, S. Geiger, T. Li, J.-P. Grote, K. Schweinar, S. Zhang, C. Scheu, D. Raabe, S. Cherevko, B. Gault and K. J. J. Mayrhofer, *Energy Environ. Sci.*, 2019, **12**, 3548-3555.
42. O. Kasian, J. P. Grote, S. Geiger, S. Cherevko and K. J. J. Mayrhofer, *Angew. Chem. Int. Ed. Engl.*, 2018, **57**, 2488-2491.
43. S. Cherevko, A. R. Zeradjanin, A. A. Topalov, N. Kulyk, I. Katsounaros and K. J. J. Mayrhofer, *ChemCatChem*, 2014, **6**, 2219-2223.
44. M. K. Debe, A. K. Schmoeckel, G. D. Vernstrom and R. Atanasoski, *J. Power Sources*, 2006, **161**, 1002-1011.
45. S. Cherevko, N. Kulyk and K. J. J. Mayrhofer, *Nano Energy*, 2016, **29**, 275-298.

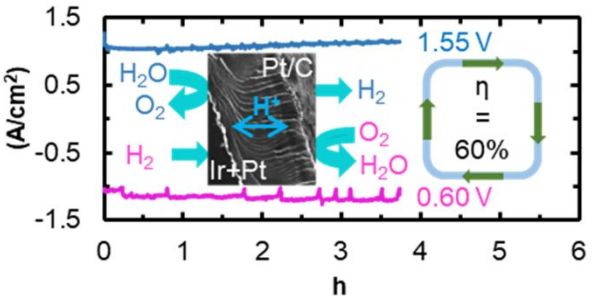

Unitized regenerative fuel cells with oxygen reactions occurring on different catalyst layers can achieve 60% round trip efficiencies at 1 A/cm^2.